THE JOURNAL OF BIOLOGICAL CHEMISTRY VOL. 287, NO. 28, pp. 23318–23331, July 6, 2012
© 2012 by The American Society for Biochemistry and Molecular Biology, Inc. Published in the U.S.A.

Expression of a Truncated Form of the Endoplasmic Reticulum Chaperone Protein, σ1 Receptor, Promotes Mitochondrial Energy Depletion and Apoptosis*[S]

Received for publication, February 3, 2012, and in revised form, May 10, 2012 Published, JBC Papers in Press, May 22, 2012, DOI 10.1074/jbc.M112.349142

Norifumi Shioda[‡], Kiyoshi Ishikawa[‡], Hideaki Tagashira[‡], Toru Ishizuka[§], Hiromu Yawo[§], and Kohji Fukunaga[‡1]

From the [‡]Department of Pharmacology, Graduate School of Pharmaceutical Sciences, Tohoku University, Sendai 980-8578 and the [§]Department of Developmental Biology and Neuroscience, Tohoku University Graduate School of Life Sciences, Sendai 980-8577, Japan

Background: An ER-associated chaperone protein, σ1 receptor (σ_1R), regulates ER/mitochondrial Ca^{2+} mobilization through the IP_3 receptor.
Results: We identify a novel short splicing variant of σ_1R, termed σ_1SR, and demonstrate its dominant negative function.
Conclusion: σ_1SR interferes with σ_1R function in mitochondrial Ca^{2+} mobilization and ATP production under ER stress conditions.
Significance: In contrast to σ_1R function, σ_1SR has detrimental effects on cell survival.

The σ1 receptor (σ_1R) regulates endoplasmic reticulum (ER)/mitochondrial interorganellar Ca^{2+} mobilization through the inositol 1,4,5-trisphosphate receptor (IP_3R). Here, we observed that expression of a novel splice variant of σ_1R, termed short form σ_1R (σ_1SR), has a detrimental effect on mitochondrial energy production and cell survival. σ_1SR mRNA lacks 47 ribonucleotides encoding exon 2, resulting in a frameshift and formation of a truncated receptor. σ_1SR localizes primarily in the ER at perinuclear regions and forms a complex with σ_1R but not with IP_3R in the mitochondrion-associated ER membrane. Overexpression of both σ_1R and the truncated isoform promotes mitochondrial elongation with increased ER mitochondrial contact surface. σ_1R overexpression increases the efficiency of mitochondrial Ca^{2+} uptake in response to IP_3R-driven stimuli, whereas σ_1SR overexpression reduces it. Most importantly, σ_1R promotes ATP production via increased mitochondrial Ca^{2+} uptake, promoting cell survival in the presence of ER stress. By contrast, σ_1SR suppresses ATP production following ER stress, enhancing cell death. Taken together, the newly identified σ_1SR isoform interferes with σ_1R function relevant to mitochondrial energy production under ER stress conditions, promoting cellular apoptosis.

Endoplasmic reticulum (ER)[2]/mitochondrial Ca^{2+} transport contributes to many cellular processes, including ATP generation and cell survival (1, 2). ER inositol 1,4,5-trisphosphate receptors (IP_3Rs) are localized in the mitochondrion-associated ER membrane (MAM) (3, 4), where the IP_3R plays critical roles in mitochondrial Ca^{2+} transport. Ca^{2+} overload through IP_3R promotes apoptosis under pathological conditions (5). By contrast, mitochondrial Ca^{2+} uptake through IP_3R is crucial for basal mitochondrial ATP production required to maintain normal cellular biogenesis (6).

Mitochondrial Ca^{2+} uptake derived from IP_3R-mediated Ca^{2+} release is facilitated by interaction between IP_3R and voltage-dependent anion channels in the MAM (4, 7, 8), and several IP_3R-binding molecular chaperones regulate mitochondrial Ca^{2+} influx from the ER (9). Among them, the σ1 receptor (σ_1R), which was cloned by Hanner *et al.* (10), was recently identified as an ER-associated chaperone protein (11). σ_1R can also translocate from the ER to the MAM or plasma membrane to modulate diverse cellular activities, including lipid metabolism (12) and *N*-methyl-D-aspartate receptor activity (13). Functional analyses in Chinese hamster ovary (CHO) cells reveal that the σ_1R stabilizes the conformation of the MAM-associated IP_3R type-3 in the ER, positively regulating Ca^{2+} influx into mitochondria. In addition, σ_1R knockdown in CHO cells facilitates ER stress-induced cell death (11).

Ca^{2+} transport between the ER and mitochondria plays important roles in neurodegenerative diseases, such as Alzheimer, Parkinson, and Huntington disease (14). Indeed, σ_1R ligands are considered therapeutic targets for several psychiatric and neurodegenerative diseases (15–17). However, how these ligands mediate neuroprotective effects remains

* This work was supported by a grant-in-aid for scientific research on innovative areas (Foundation of Synapse and Neurocircuit Pathology), Grants-in-aid for Scientific Research from the Ministry of Education, Science, Sports and Culture of Japan and Core Research for Evolutional Science and Technology, Japan Science and Technology Agency, 22390109 and 24659024 (to K. F.) and 23790072 and 23110501 (to N. S.), and from the Smoking Research Foundation (to K. F.).

[S] This article contains supplemental Figs. 1–4 and Table 1.

The nucleotide sequence(s) reported in this paper has been submitted to the GenBank™/EBI Data Bank with accession number(s) AB721301.

[1] To whom correspondence should be addressed: Dept. of Pharmacology, Graduate School of Pharmaceutical Sciences, Tohoku University, 6-3 Aramaki-Aoba Aoba-ku, Sendai 980-8578, Japan. Tel.: 81-22-795-6836; Fax: 81-22-795-6835; E-mail: kfukunaga@m.tohoku.ac.jp.

[2] The abbreviations used are: ER, endoplasmic reticulum; ALS, amyotrophic lateral sclerosis; ATP5A1, ATP synthase; IP_3, inositol 1,4,5-trisphosphate; IP_3R, inositol 1,4,5-trisphosphate receptor; MAM, mitochondrion-associated ER membrane; Mfn2, Mitofusin-2; PACS-2, phosphofurin acidic cluster sorting protein 2; PERK, RNA-dependent protein kinase-like ER kinase; σ_1SR, short form σ1 receptor; σ_1R, σ1 receptor; mt, mitochondrial; ICM, intracellular like medium; eGFP, enhanced GFP; erRFP, ER-targeted RFP.

unclear. More recently, σ_1R mutations have been observed in patients with dementia attributable to frontotemporal lobar degeneration (18) or juvenile amyotrophic lateral sclerosis (19). Interestingly, the latter apparently promotes nuclear transport of mutant forms of σ_1R.

In this study, we observed a novel σ_1R splicing variant in mouse brain, namely a short form (σ_1SR) lacking 47 bp of exon 2. σ_1SR protein is primarily expressed in the ER, where it interacts with σ_1R. Interestingly, σ_1SR overexpression decreased mitochondrial Ca^{2+} uptake in response to IP_3R-mediated stimulation, indicating that it antagonizes σ_1R activity. Moreover, σ_1SR overexpression promoted autophagic apoptosis, consistent with IP_3R destabilization and decreased ATP production attributable to reduced mitochondrial Ca^{2+} uptake. Our results show for the first time that σ_1SR interferes with mitochondrial ATP biogenesis by inhibiting σ_1R function following ER stress.

EXPERIMENTAL PROCEDURES

Sequencing and Construction of Expression Vectors Encoding σ_1R Isoforms—Total RNAs were prepared from mouse brain hippocampus using TRIzol LS reagent (Invitrogen) according to the manufacturer's protocol. mRNA was reverse-transcribed into single-stranded cDNA using an oligo(dT) primer (Promega, Madison, WI) and Moloney murine leukemia virus-reverse transcriptase (Invitrogen). DNA sequences of σ_1R isoforms amplified by PCR using specific 5′- and 3′-primers and primer sequences are shown in supplemental Table 1. All DNA sequences were determined at the Fasmac DNA Sequence Service (FASMAC Co., Ltd., Atsugi, Japan). To construct expression vectors, PCR amplification products were digested with XhoI and BamHI and ligated with purified XhoI- and BamHI-digested pmCherry-N1 or pEGFP-N1 vector (Clontech) in the sense orientation.

Cell Culture, Transfection, and Production of Stably Transfected Cell Lines—Neuro-2a cells from a mouse neuroblastoma C1300 tumor were obtained from the Human Science Research Resources Bank (IFO50081) (Osaka, Japan). Neuro-2a cells were grown in Dulbecco's minimal essential medium (DMEM) supplemented with 10% heat-inactivated fetal bovine serum (FBS) and penicillin/streptomycin (100 units/100 μg/ml) in a 5% CO_2 incubator at 37 °C. Cells were transfected with expression vectors using Lipofectamine 2000 (Invitrogen), and experiments were performed 48 h later as described (20). σ_1R small interfering (si)RNA (sense, 5′-ACACGTGGATGGTGGAGTA-3′, and antisense, 5′-TACTCCACCATCCACGTGT-3′) was purchased from Exigen (Tokyo, Japan). Transfections were performed with 100 nM σ_1Rs siRNA according to the methods of Ref. 21. Stably transfected Neuro-2a cells were prepared as described (22). Briefly, cells were transfected with σ_1R or σ_1SR cDNA in pmCherry-N1 expression vectors as described above. Transfected cells were plated in medium containing 1000 μg G418/ml, and G418-resistant colonies were isolated.

Immunoprecipitation and Immunoblotting—Immunoprecipitation and immunoblotting analysis were performed as described (20). 12-Week-old male C57BL/6J mouse brains were immediately removed from euthanized mice and perfused in ice-cold buffer for 3 min (0.32 M sucrose, 20 mM Tris-HCl, pH 7.4), and olfactory bulb, cortex, hippocampus, striatum, and brainstem were dissected. These samples and Neuro-2a cells were homogenized in buffer containing 50 mM Tris-HCl, pH 7.4, 0.5% Triton X-100, 0.5 M NaCl, 4 mM EDTA, 4 mM EGTA, 1 mM Na_3VO_4, 50 mM NaF, 1 mM DTT, 2 μg/ml pepstatin A, and 1 μg/ml leupeptin, then treated with Laemmli sample solution, and boiled for 3 min. Antibodies included the following: rabbit polyclonal antibodies against the N-terminal cytosolic domain (52–69 amino acids) (1:1000) and C-terminal lumenal domain (143–165 amino acids) of σ_1R (1:1000; a kind gift of Dr. Teruo Hayashi, NIDA, Baltimore); GFP (1:2000; Clontech); calcineurin (1:1000) (23); voltage-dependent anion channel (1:1000; Cell Signaling Technology, Beverly, MA); CREB-2 (1:200; Santa Cruz Biotechnology, Santa Cruz, CA); LC-3 (PM036, 1:1000; MBL, Nagoya, Japan); rabbit monoclonal antibody against phospho-PERK (1:1000; Cell Signaling Technology); mouse monoclonal antibodies against C/EBP homologous protein (1:200; Santa Cruz Biotechnology); β-tubulin (1:1000; Sigma); and pan-IP_3R (1:500; Millipore, Bedford, MA). For subcellular fractionation, cells were washed twice with ice-cold phosphate-buffered saline (PBS), separated into cytosolic, ER, and mitochondrial membranes and nuclear fractions using the subcellular protein fractionation kit (Thermo Fisher Scientific Inc., Waltham, MA) following the manufacturer's protocol, and analyzed by Western blot analysis.

Immunohistochemistry—Fluorescence immunohistochemical studies were performed as described (24). Cells were fixed in 4% paraformaldehyde in phosphate buffer for 30 min at room temperature and washed in PBS. Cells were blocked with 3% bovine serum albumin in PBS for 1 h. First antibodies included mouse monoclonal antibodies against GM130 (1:1000; BD Biosciences) and rabbit polyclonal antibody against LC-3 (PM036, 1:1000; MBL). After thorough washes in PBS, sections were incubated with secondary antibodies in blocking solution at 20 °C for 24 h. Antibodies included Alexa 594-labeled anti-mouse IgG and Alexa 448-labeled anti-rabbit IgG (1:500; Invitrogen) in blocking solution at 20 °C for 3 h. After several washes in PBS, sections were mounted on slides with Vectashield (Vector Laboratories Inc., Burlingame, CA). For nuclear staining, sections were incubated with DAPI (Vector Laboratories, Burlingame, CA). Immunofluorescent images were analyzed using a confocal laser scanning microscope (LSM700; Zeiss, Thornwood, NY). To detect ER and mitochondrial distribution, Neuro-2a cells were transfected with erRFP or mitochondrial GFP (mtGFP) (Bacman 2.0, Invitrogen) and analyzed using confocal microscopy of fixed cells.

Morphometric and Contact Analysis—Morphometric and contact analysis was performed as described previously (25) with modifications. For morphometric analysis of mitochondria, the major axis length of each identified object was calculated. Cells were scored as showing elongated mitochondria when >50% of the objects in the image displayed a major axis longer than 3 μm. For morphometric analysis of ER, major axis length and elongation index of each identified object were calculated. Cells were scored as showing reticular ER when the major axis was longer than 5 μm, and the elongation index exceeded 4 in more than 50% of the identified objects. For mitochondrial network and ER co-localization, one focal plane was

analyzed. Images were deconvoluted, and background was subtracted using ImageJ software. Co-localization of organelles was quantified using the co-localization coefficient of Manders *et al.* (26).

Quantification of Neurite Sprouting—Neurite sprouting by Neuro-2a cells was assessed by staining with βIII-tubulin (1:1000, Promega, Madison, WI) and use of the VECTASTAIN ABC kit (Vector Laboratories, Burlingame, CA), according to the manufacturer's protocol. Images were acquired using the 40× objective of a microscope (BX51WI, Olympus, Tokyo, Japan) equipped with a digital camera (Micropublisher 5.0, QIMAGING, Burnaby, British Columbia, Canada). Sprouting was quantified as the percentage of cells with neurites longer than twice the body diameter. Neurite length was determined using ImageJ software. Six fields (100 cells per field) in each condition were chosen randomly and photographed.

Fluorometric $[Ca^{2+}]_c$ and $[Ca^{2+}]_{mt}$ Measurements—Neuro-2a cells were grown on 0.01% poly-L-lysine (Sigma)-coated glass-bottom dishes. For $[Ca^{2+}]_c$ measurement, cells were rinsed in Krebs buffer (135 mM NaCl, 6 mM KCl, 1.2 mM $MgCl_2$, 12 mM glucose, 1.5 mM $CaCl_2$, 12 mM HEPES, pH 7.3), loaded with 2.5 μM Fura-2/AM (Sigma) for 15 min at 37 °C in darkness, and washed with Krebs buffer for 15 min. Measurements were performed in Ca^{2+}-free Krebs buffer including 2 mM EGTA. Ratio measurements were performed every 3 s by excitation at 340 and 380 nm and recording of the emission at 530 nm. Ratio values were derived by averaging fluorescence intensity from the entire cytosolic area. To measure $[Ca^{2+}]_{mt}$, cells were transfected with the ratiometric pericam (a kind gift of Dr. Atsushi Miyawaki, RIKEN Brain Science Institute, Wako-City, Japan) targeted to the mitochondrial matrix. Two days later, cells were exposed to externally applied 10 μM ATP in Ca^{2+}-free Krebs buffer and imaged. Cells were permeabilized by exposure to intracellular like medium (ICM) (125 mM KCl, 19 mM NaCl, 10 mM HEPES-KOH, pH 7.3, 1 mM EGTA) and appropriate concentrations of $CaCl_2$ (330 μM $CaCl_2$ for 50 nM free Ca^{2+}) (27) containing 250 μg/ml (w/v) saponin (MP Biomedicals, Ohio) for 3 min. Permeabilized cells were washed with ICM and then exposed to ICM containing 1 μM inositol 1,4,5-trisphosphate (IP_3) (Biomol, Plymouth Meeting, PA). Dual excitation imaging with ratiometric pericam-mt required two filters (excitation 482/35, dichroic mirror 506, emission 536/40 and excitation 414/46, dichroic mirror 510, emission 527/20). $[Ca^{2+}]_c$ and $[Ca^{2+}]_{mt}$, which were monitored during the assay on an inverted microscope (Leica DM IRB, Japan), were equipped with CCD cameras (ORCA-ER; Hamamatsu, Japan). Captured images were analyzed using the Metafluor imaging system (Molecular Devices, Sunnyvale, CA).

Drug Treatments—ER stress was induced by treatment of cells with 2 μg/ml tunicamycin (Sigma) for 4 or 24 h. For cell viability experiments, tunicamycin treatment continued for 48 h. Mitochondrial Ca^{2+} uptake was inhibited by 10 μM Ru360 (Calbiochem).

ATP Measurement—Cells were plated in 6-cm plates, and ATP content was determined using luciferin and a luciferase assay kit (Toyo B-net, Tokyo, Japan) following the manufacturer's protocol.

TUNEL Staining—DNA fragmentation and apoptotic bodies were detected by the TUNEL method using an *in situ* apoptosis detection kit (Takara Bio Inc., Shiga, Japan), as described (28). One hundred cells from 13 randomly selected fields were counted in each experiment.

Quantification of mRNA by Real Time PCR—Real time PCR analysis was performed as described (24) in 48-well plates (Mini Opticon Real Time PCR System, Bio-Rad) using iQ SYBR Green Supermix 2× (Bio-Rad). Primer sequences are shown in supplemental Table 1. Relative quantities of target mRNAs were determined by the comparative threshold cycle (Δ*CT*) method and normalized to GAPDH quantity. Product purity and specificity were confirmed by omitting the template and performing a standard melting curve analysis.

Statistical Evaluation—All values were expressed as means ± S.E. Comparison between two experimental groups was made using the unpaired Student's *t* test. Statistical significance for differences among groups was tested by one-way analysis of variance, followed by multiple comparisons between control and other groups using Dunnett's multiple comparison test. $p < 0.05$ was considered significant.

RESULTS

Identification of a Novel σ_1R Splicing Variant—σ_1R, a non-opioid receptor (29, 30), was previously cloned from guinea pigs (10), humans (31), and mice (32). All forms showed greater than 80% amino acid homology but no structural homology with any other receptor family. We screened a mouse hippocampal cDNA library by PCR using primer sets derived from the coding region of mouse *Sigmar1* (Fig. 1*A*, *p1* and *p2*) and identified the *Sigmar1*-coding sequence fragment (Fig. 1*B*, *lane 1*) and a novel smaller fragment (Fig. 1*B*, *lane 2*). When we amplified what would be an ~200-bp fragment spanning σ_1R exon 2 to exon 3 (Fig. 1*A*, *p3* and *p4*) from the *Sigmar1*-coding sequence fragment, we detected the expected 200-bp fragment (Fig. 1*B*, *lane 3*) and also an ~150-bp fragment (Fig. 1*B*, *lane 4*). Sequencing analysis revealed that the short fragment lacks 47 bp from exon 2 of the full-length gene. We subsequently identified a novel 231-bp splicing variant of σ_1R and called it σ_1SR (Fig. 1*B*, *lane 5*). A human sequence corresponding to mouse σ_1SR had been deposited in GenBank™ under accession number BC007839.2. (Fig. 1*C*, *left*), but protein expression and function had not been evaluated. Our analysis indicated that the novel splice conformed to the G(T/A)G rule (Fig *1D*) and that splicing of the 47-bp fragment caused a frameshift starting at amino acid 103 and translation termination due to a newly generated stop codon. The predicted primary structure of σ_1SR contains 106 rather than the 223 amino acids seen in σ_1R. The first 102 amino acids of both proteins are identical, but the C-terminal four residues of σ_1SR differ from the longer form, because they are derived from translation of the frame-shifted σ_1R exon 3 (Fig. 1, *C* and *D*).

Tissue Distribution and Localization of Both σ_1R Isoforms—To investigate tissue distribution and relative expression levels of σ_1R and σ_1SR, we performed immunoblot analysis in adult mouse brain using antibodies against the σ_1R N-terminal cytosolic domain (amino acids 52–69) or the C-terminal lumenal domain (amino acids 143–165). To confirm endogenous

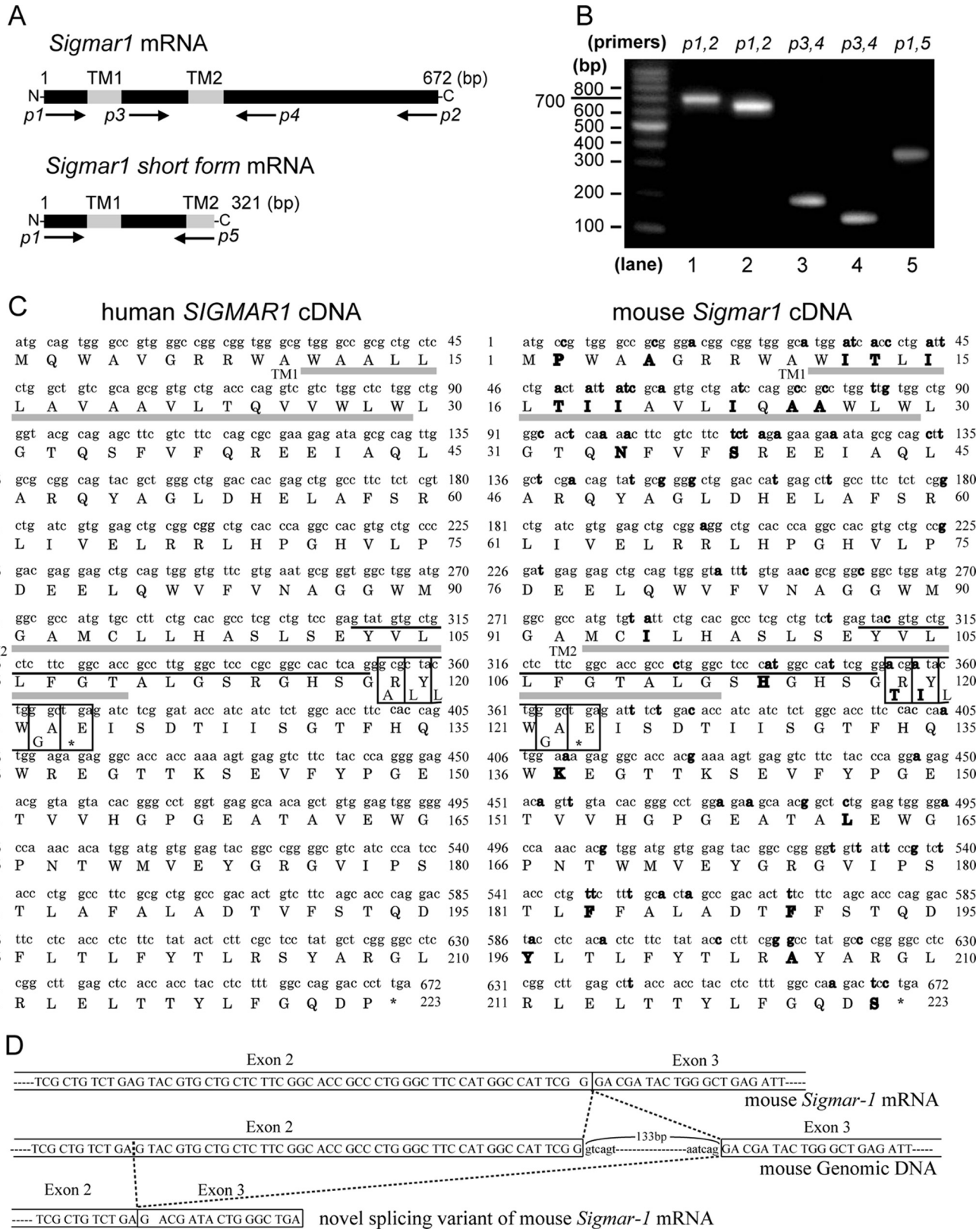

FIGURE 1. **σ_1R alternative splicing.** *A,* position of PCR primers relative to receptor sequences (transmembrane domain). *B,* PCR of an adult mouse brain hippocampus cDNA library was performed using the indicated oligonucleotide primers. *C,* sequence of coding region of human *SIGMAR1* (*left*) and mouse *Sigmar1* (*right*) cDNA. The deduced amino acid sequence is presented using the one-letter code. Differences between homologues are shown in *bold*. Two putative transmembrane domains (TM1 and TM2) are shown in *gray underlines*, and the 47-bp of sequences deleted from full-length σ_1R are shown in *black underlines*. Their deletion results in a frameshift, giving rise to four novel amino acids in σ_1SR (*boxed*). *D,* proposed splicing mechanism of σ_1Rs. Exons are *outlined*, and coding sequence is denoted by *capital letters*. Intronic sequence is denoted by *lowercase letters*.

expression of σ_1R and σ_1SR, we observed immunoreactive bands in cell extracts from neuroblastoma Neuro-2a cells transfected with both cDNAs (Fig. 2*A*, *lanes 3–8*). Using an N-terminal cytosolic domain-specific antibody, we observed marked variation in the ratio of endogenous σ_1SR (seen as a 12-kDa band) to σ_1R (seen as a 26-kDa band) protein in the mouse brain regions tested (Fig. 2*A*, *upper panel, lanes 9–13*). An unidentified protein of the 19-kDa protein was observed in the hippocampus and brainstem lysates. As expected, a C-terminal lumenal domain antibody detected an immunoreactive σ_1R band but not σ_1SR (Fig. 2*A*, *lower panel, lanes 9–13*). σ_1SR protein levels were high in cortex, hippocampus, and striatum

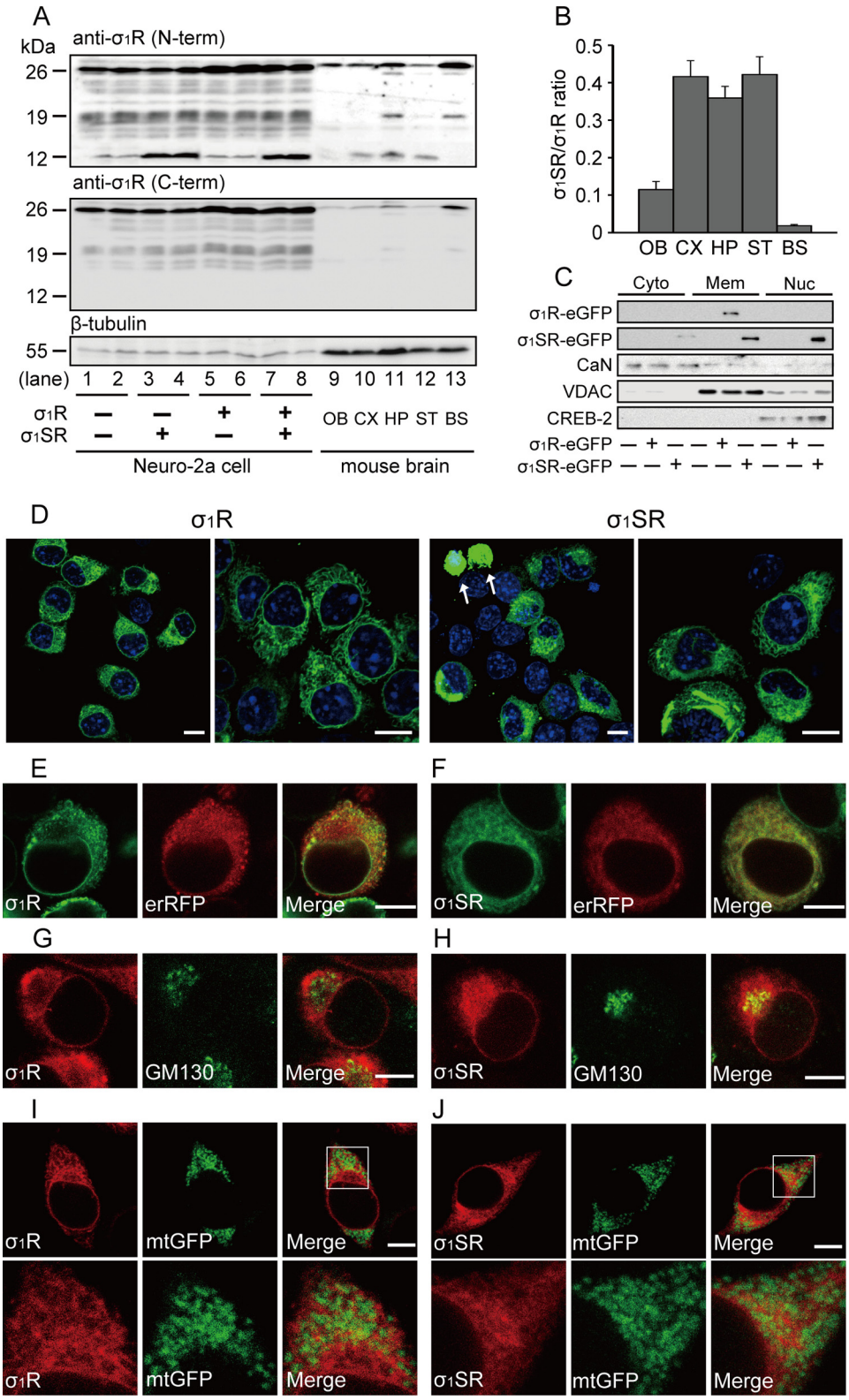

(σ_1SR/σ_1R ratio of 0.4) but barely detectable in olfactory bulb and brainstem (Fig. 2*B*). To further investigate differences in subcellular localization, we fractionated lysates of Neuro-2a cells transfected with 3′ eGFP-tagged σ_1R (σ_1R-eGFP) or σ_1SR (σ_1SR-eGFP) cDNA into cytosolic, ER, and mitochondrial membrane (including MAM) and nuclear fractions. High levels of σ_1R-eGFP were found in ER and mitochondrial membrane fractions, and relatively low levels were seen in other fractions, whereas σ_1SR-eGFP was detected in membrane and nuclear fractions (Fig. 2*C*). To determine subcellular localization of these proteins, we undertook confocal microscopy of fluorescence-tagged σ_1R and σ_1SR in Neuro-2a cells. σ_1R-eGFP and σ_1SR-eGFP were primarily observed in perinuclear regions, although low levels of fluorescence were seen in the nuclei of σ_1SR-eGFP-expressing cells (Fig. 2*D*). A punctate perinuclear staining pattern of erRFP, which targets and serves as a marker of endoplasmic reticulum, largely co-localized with σ_1R-eGFP (Fig. 2*E*) and σ_1SR-eGFP (Fig. 2*F*). Interestingly, the Golgi marker GM130 showed considerable co-localization with σ_1SR-eGFP (Fig. 2*H*) but not with σ_1R-eGFP (Fig. 2*G*). Both mCherry-tagged σ_1R isoforms were detected in some overlays with the mitochondrial marker mtGFP, suggesting that σ_1SR protein also localizes on MAMs, as reported for σ_1R (Fig. 2, *I* and *J*) (11). These results suggest that the subcellular distribution of both σ_1R isoforms is similar, although σ_1SR is also seen in the Golgi apparatus and nucleus.

Overexpression of Either σ_1R Isoform Promotes Mitochondrial Elongation and Increases ER/Mitochondrial Contact Space—Based on their subcellular location, we analyzed the role of both σ_1R isoforms in ER and mitochondrial morphology and in ER/mitochondria interaction. σ_1R or σ_1SR overexpression did not alter the reticular ER structure of erRFP-infected Neuro-2a cells (Fig. 3*B*; 89.1 ± 2.8% in control, 88.7 ± 2.9% in σ_1R-, and 83.6 ± 3.6% in σ_1SR-transfected cells). However, expression of either isoform alone promoted mitochondrial elongation, as shown by three-dimensional reconstruction of mitochondrion-targeted green fluorescent protein (Fig. 3*C*; 41.6 ± 7.5% in control, 77.4 ± 7.0% in σ_1R-, and 67.3 ± 8.9% in σ_1SR-transfected cells). In addition, confocal semiquantitative analysis of ER/mitochondria juxtaposition showed that tethering of ER and mitochondria increased either isoform expressed in Neuro-2a cells (Fig. 3*D*; 2.6 ± 0.3% in controls, 4.6 ± 0.9% in σ_1R-, and 3.8 ± 0.7% in σ_1SR-transfected cells).

σ_1SR Forms a Complex with σ_1R but Not with IP_3Rs—Because both σ_1R isoforms are similarly distributed, we asked whether either directly interacted with IP_3Rs. To do so, we performed immunoprecipitation of extracts from σ_1SR-mCherry-expressing cells co-expressing σ_1R-eGFP using an eGFP antibody followed by immunoblotting with an anti-σ_1R N-terminal cytosolic domain-specific antibody. We observed an immunoreactive σ_1SR-mCherry band (41 kDa) (Fig. 4*A*, *upper panel, lane 9*) not seen in immunoprecipitates from extracts from eGFP-, σ_1R-eGFP-, or σ_1SR-mCherry-overexpressing cells (Fig. 4*A*, *upper panel, lanes 6–8*). Immunoreactive bands with molecular masses corresponding to two fluorescence-tagged σ_1R isoforms of 55 and 41 kDa were detected in each cell extract (Fig. 4*A*, *lanes 2–4*). To confirm the specificity of fluorescence-tagged σ_1SR bands, we used an anti-σ_1R C-terminal lumenal domain-specific antibody. σ_1SR-eGFP (37 kDa) and σ_1SR-mCherry (41 kDa) bands were not detected (Fig. 4*A*, *lower panel*).

Because σ_1R forms a complex with IP_3R type-3 in CHO cells (11), we examined potential binding of σ_1R and σ_1SR with IP_3R in Neuro-2a cells. After immunoprecipitation with an IP_3R antibody, we observed only a 26-kDa σ_1R immunoreactive band in σ_1R- or σ_1SR-overexpressing cells (Fig. 4*B*, *lanes 4–6*). Next, after σ_1R immunoprecipitation with an anti-σ_1R N-terminal specific antibody, we undertook immunoblotting using an anti-IP_3Rs antibody. As expected, increased levels of an IP_3R immunoreactive band were seen in σ_1R-overexpressing (Fig. 4*C*, *lane 5*) but not σ_1SR-overexpressing (Fig. 4*C*, *lanes 4* and *6*) cells relative to controls. No significant differences in IP_3R protein expression were observed between control cells and cells expressing σ_1R isoforms (Fig. 4*C*, *lanes 1–3*). Confocal microscopy of Neuro-2a cells indicated that σ_1SR-mCherry coincided with σ_1R-GFP immunofluorescence in the ER (Fig. 4*D*).

σ_1SR Expression Reduces Mitochondrial Ca^{2+} Uptake in Response to IP_3R-driven Stimuli—IP_3Rs are important for ER-mitochondrial Ca^{2+} transport, which is regulated by σ_1R in the MAM of CHO cells (11). Because σ_1SR forms a complex with σ_1R, we assessed a potential role for σ_1SR in mitochondrial Ca^{2+} uptake. To assay mitochondrial Ca^{2+} uptake in Neuro-2a cell lines stably expressing σ_1R-mCherry (σ_1R-mCh cells) or σ_1SR-mCherry (σ_1SR-mCh cells), we conducted Ca^{2+} imaging using ratiometric pericam-mt Ca^{2+} probes, which localize to mitochondria (Fig. 5*A*) (33). We confirmed that σ_1R- and σ_1SR-mCherry mRNA levels in each line were equivalent, and we also found that levels showed an approximate 20-fold increase over parental Neuro-2a cells (supplemental Fig. 1*A*).

We then asked whether mitochondrial Ca^{2+} elevation elicited by ATP, acting on receptors coupled with G_q protein to stimulate IP_3 production. For this experiment, Ca^{2+}-free Krebs buffer containing 2 mM EGTA was used to assess intracellular Ca^{2+} mobilization and mitochondrial Ca^{2+} elevation through

FIGURE 2. **Tissue distribution and localization of σ_1Rs.** *A,* representative immunoblots probed with antibodies against the σ_1R N-terminal cytosolic domain (*upper panel*) or the C-terminal lumenal domain (*lower panel*). As control bands, extracts from Neuro-2a cells transfected with σ_1R and σ_1SR constructs (*lanes 1–8*) are shown. *B,* quantitative densitometry shows the ratio of σ_1SR to σ_1R protein expression among different brain regions. *OB,* olfactory bulb; *CX,* cortex; *HP,* hippocampus; *ST,* striatum; *BS,* brainstem. $n = 4$ in each group. *C,* cytosolic (*Cyto*), ER, mitochondrial membrane (*Mem*), and nuclear (*Nuc*) fractions from eGFP tagged-σ_1R isoform-transfected Neuro-2a cells were blotted with antibodies against GFP, calcineurin (*CaN*, cytosolic marker), voltage-dependent anion channel (ER and mitochondrial membrane marker), and CREB-2 (nuclear marker). *D–I,* σ_1R localization in Neuro-2a cells. Confocal images show co-localization of fluorescence (eGFP or mCherry)-tagged-σ_1R isoforms and markers of ER (erRFP), Golgi apparatus (GM130), and mitochondria (mtGFP). *D,* σ_1R-eGFP (*left*) and σ_1SR-eGFP (*right*) are mainly expressed in perinuclear regions. A small number of GFP aggregates are detected in nuclei of σ_1SR-eGFP-expressing cells (shown by *arrow*). *Right panels* are high magnification images. *E* and *F*, immunoreactivity of both σ_1R-eGFP isoforms (*green*) and erRFP (*red*) almost completely merge. *G* and *H,* GM130 (*green*) immunoreactivity co-localizes with σ_1SR-mCherry (*H*) (*red*) but not with σ_1R-mCherry (*G*) (*red*). *I* and *J,* both mCherry-tagged σ_1R isoforms (*red*) were detected in a few overlays with the mitochondrial marker mtGFP (*green*). *Lower panels* in *I* and *J* are high magnification images. *Scale bars,* 10 μm.

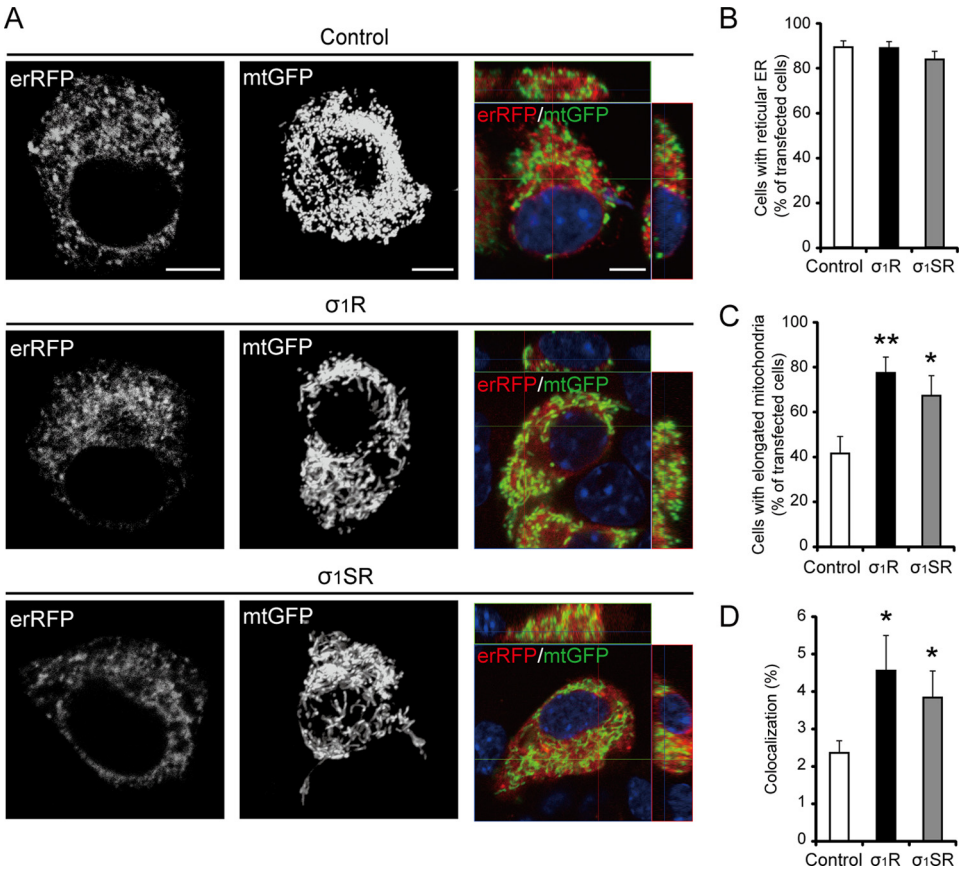

FIGURE 3. **Both σ_1R isoforms regulate mitochondrial morphology and juxtaposition of the ER to mitochondria.** *A,* representative images of three-dimensional reconstructions of ER (erRFP; *left*), mitochondria (mtGFP; *middle*), and merged images showing ER and mitochondria co-localization (*yellow*; *right*). *B,* morphometric analysis of ER shape in cells transfected with erRFP ($n = 3$, 18 cells per experiment). *C,* quantitative analysis of mitochondrial shape in cells transfected with mtGFP ($n = 4$, 12 cells per experiment). *D,* quantitative analysis of co-localization of ER and mitochondria (as a percentage of total mitochondrial volume) in cells co-transfected with erRFP and mtGFP ($n = 4$, 20 cells per experiment). Each *bar* represents the mean ± S.E. *, $p < 0.05$; **, $p < 0.01$ *versus* control cells. *Scale bar,* 10 μm.

the ER IP_3R. As shown in Fig. 5*B*, ATP stimulation caused a rapid rise in $[Ca^{2+}]_{mt}$, followed by a gradual decline with a sustained plateau phase in control cells (*black line*). In σ_1R-mCh cells (Fig. 5*B*, *red line*), the $[Ca^{2+}]_{mt}$ increase was markedly enhanced compared with that seen in control cells, although it was significantly decreased in σ_1SR-mCh cells (*blue line*). Interestingly, decreased $[Ca^{2+}]_{mt}$ mobilization seen in σ_1SR-mCh cells was significantly rescued to levels comparable with those seen in control cells by σ_1R co-expression (Fig. 5*B*, *green line*). Peak amplitudes of $[Ca^{2+}]_{mt}$ mobilization are summarized (0.18 ± 0.02 in control, 0.3 ± 0.01 in σ_1R-mCh, 0.09 ± 0.02 in σ_1SR-mCh, and 0.14 ± 0.01 in σ_1SR-mCh plus σ_1R expression).

To confirm that IP_3Rs function in $[Ca^{2+}]_{mt}$ mobilization, saponin-permeabilized cells were treated with IP_3, and $[Ca^{2+}]_{mt}$ was monitored in the presence of ICM buffer. Consistent with results seen after ATP application, IP_3-mediated $[Ca^{2+}]_{mt}$ mobilization was significantly enhanced in σ_1R-mCh cells and decreased in σ_1SR-mCh cells relative to control cells. In addition, $[Ca^{2+}]_{mt}$ decreases seen in σ_1SR-mCh cells were rescued by σ_1R co-expression (Fig. 5*C*; peak amplitude 0.17 ± 0.04 in control cells, 0.22 ± 0.04 in σ_1R-mCh cells, 0.13 ± 0.03 in σ_1SR-mCh cells, and 0.19 ± 0.06 in σ_1SR-mCh plus σ_1R expression).

We next examined intracellular mobilization $[Ca^{2+}]_c$ following ATP stimulation using the ratiometric indicator Fura-2/AM in Ca^{2+}-free Krebs buffer. Interestingly, ATP-induced $[Ca^{2+}]_c$ mobilization in σ_1R-mCh cells was significantly reduced compared with controls. By contrast, $[Ca^{2+}]_c$ mobilization in σ_1SR-mCh cells was greater than that seen in control cells and that increase was suppressed by σ_1R co-expression (Fig. 5*D*; peak amplitude 0.13 ± 0.02 in control cells, 0.12 ± 0.08 in σ_1R-mCh cells, 0.16 ± 0.06 in σ_1SR-mCh cells, and 0.1 ± 0.03 in σ_1SR-mCh plus σ_1R cells). This evidence strongly suggests that increased IP_3-mediated $[Ca^{2+}]_{mt}$ mobilization stimulated by σ_1R overexpression decreases $[Ca^{2+}]_c$ mobilization, although IP_3-mediated $[Ca^{2+}]_{mt}$ mobilization due to σ_1SR overexpression enhances it.

We also confirmed that ATP-induced $[Ca^{2+}]_{mt}$ mobilization was mediated by σ_1Rs using siRNA knockdown of both σ_1R isoforms. Expression levels of both proteins were down-regulated ~70% by siRNA treatment (supplemental Fig. 1*B*). σ_1R isoform knockdown significantly decreased ATP-induced $[Ca^{2+}]_{mt}$ mobilization (Fig. 5*E*; peak amplitude 0.18 ± 0.03 in control cells and 0.1 ± 0.02 in σ_1R isoform siRNA cells); conversely, knockdown of both σ_1R and σ_1SR protein elevated ATP-induced $[Ca^{2+}]_c$ mobilization (Fig. 5*F*; peak amplitude 0.15 ± 0.05 in control cells and 0.19 ± 0.08 in σ_1R isoform siRNA cells).

Overexpression of σ_1R-mCh and σ_1SR-mCh may alter the capacity of ER Ca^{2+} stores. To assess this possibility, we stim-

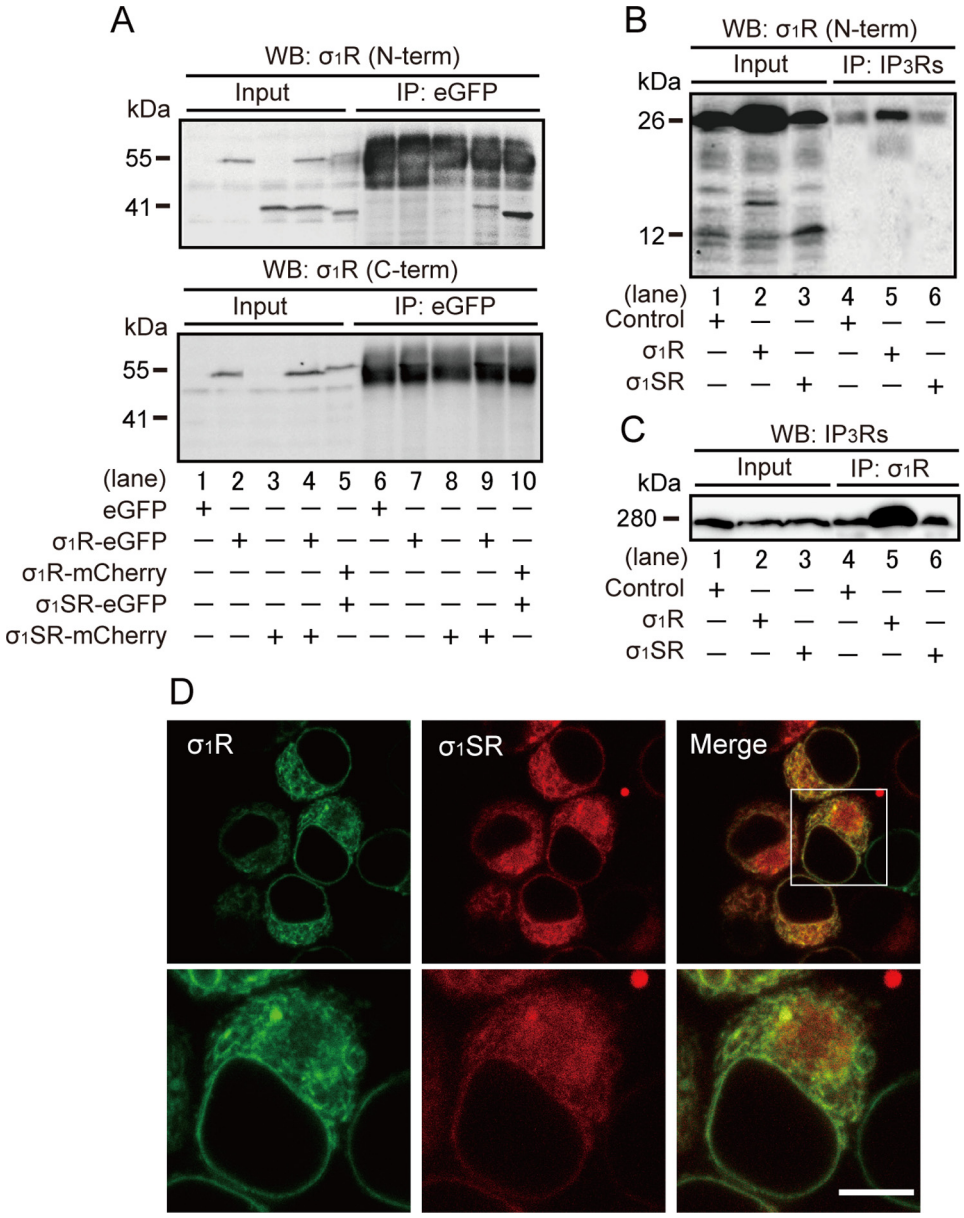

FIGURE 4. **σ_1SR forms a complex with and co-localizes with σ_1R.** *A,* co-immunoprecipitation of fluorescence-tagged σ_1SR and σ_1R in Neuro-2a cells. Extracts were immunoprecipitated (*IP*) with anti-eGFP antibody, and immunoprecipitates were immunoblotted (*WB*) with anti-σ_1R N-terminal cytosolic domain (*upper panel*) or with the C-terminal lumenal domain (*lower panel*) antibody. Cell extracts (*Input*) from Neuro-2a cells transfected with eGFP (*lane 1*), σ_1R-eGFP (*lane 2*), σ_1R-mCherry (*lane 3*), σ_1SR-eGFP (*lane 4*), or σ_1SR-mCherry (*lane 5*) constructs are shown as positive controls for σ_1R isoform immunoreactive bands. *B* and *C,* co-immunoprecipitation of σ_1Rs and IP_3Rs in Neuro-2a cells. Extracts were immunoprecipitated with anti-IP_3Rs (*B*) or anti-σ_1R N-terminal cytosolic domain (*C*) antibody, and immunoprecipitates were immunoblotted (*WB*) with anti-IP_3Rs (*B*) or anti-σ_1R N-terminal (*C*) antibody. As a positive control for σ_1Rs and IP_3Rs immunoreactive bands, cell extracts (*Input*) are shown from intact (*lane 1*) or σ_1R- (*lane 2*) or σ_1SR (*lane 3*)-transfected cells. *D,* confocal images showing co-localization of σ_1R-eGFP (*green*) and σ_1SR-mCherry (*red*) in Neuro-2a cells. *Scale bar,* 10 μm.

ulated cells with thapsigargin, an inhibitor of the sarcoplasmic reticulum calcium ATPase. Thapsigargin treatment promoted a transient increase in $[Ca^{2+}]_c$ by depleting Ca^{2+} stores in the absence of extracellular Ca^{2+}, and subsequent addition of extracellular Ca^{2+} increased $[Ca^{2+}]_c$ through capacitative Ca^{2+} entry. Both the capacity of ER Ca^{2+} stores and capacitative Ca^{2+} entry were comparable in cells with or without σ_1R and σ_1SR overexpression (supplemental Fig. 2). These results suggest that both σ_1R isoforms affect the efficiency of mitochondrial Ca^{2+} uptake in response to IP_3R-driven stimuli without changing the capacity of ER Ca^{2+} stores.

σ_1SR Acts Antagonistically to σ_1R following ER Stress—Because σ_1SR expression suppresses IP_3-mediated $[Ca^{2+}]_{mt}$ mobilization and enhances receptor-mediated $[Ca^{2+}]_c$ mobilization through the ER, we hypothesized that σ_1SR overexpression increases the vulnerability of a cell to ER stress. To test this, we evaluated the effect of the ER stressor tunicamycin on overexpression of σ_1R isoforms. Tunicamycin treatment promoted expression of both endogenous σ_1R and σ_1SR protein in σ_1R-mCh but not control cells. Conversely, tunicamycin treatment reduced expression of both endogenous σ_1R and σ_1SR in σ_1SR-mCh cells (Fig. 6*B*).

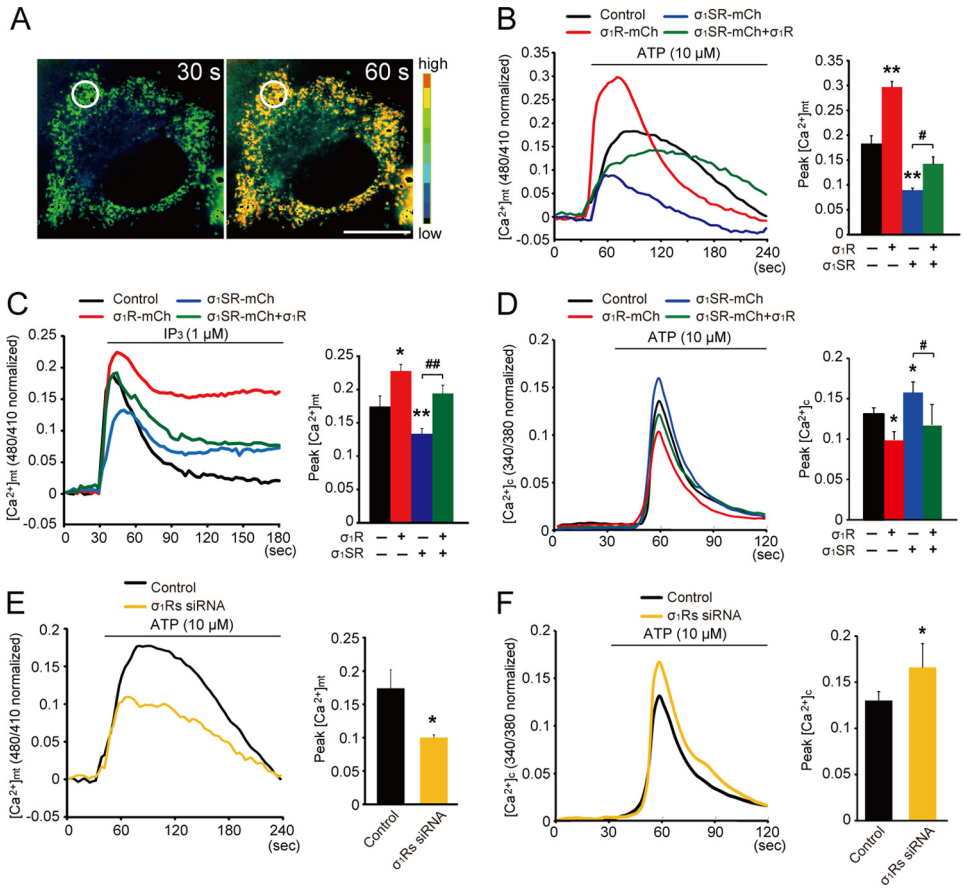

FIGURE 5. **σ_1SR expression reduces mitochondrial Ca^{2+} uptake in response to IP_3R-driven stimuli.** *A*, pseudo-colored images of Neuro-2a cells expressing the mitochondrial Ca^{2+} indicator, ratiometric pericam-mt, at 30 s (*left*) and 60 s (*right*), corresponding to a control cell in *B*. Regions of interest for $[Ca^{2+}]_{mt}$ measurement is indicated by the *circles* in *A*. *B, C,* and *E*, relative fluorescence intensity changes following treatment with 10 μM ATP in Neuro-2a cells (*B* and *E*) or 1 μM IP_3 in permeabilized Neuro-2a cells (*C*) after transfection of a mitochondrial pericam probe. *D* and *F,* relative Fura-2/AM fluorescence intensity changes following 10 μM ATP stimulation. *Top line* indicates incubation period. The ratio of the ratiometric pericam-mt and Fura-2 fluorescence peak value of the release phase relative to the preceding base line is shown on the *right*. Each *bar* represents the mean ± S.E. *, $p < 0.05$; **, $p < 0.01$ *versus* control cells. #, $p < 0.05$; ##, $p < 0.01$ *versus* σ_1SR-mCh cells. $n = 12$ cells per experiment, performed in triplicate from four preparations. *Scale bar,* 10 μm.

Tunicamycin treatment also promoted significant degradation of IP_3R proteins in control but not σ_1R-mCh cells, suggesting a chaperone activity for σ_1R. More importantly, σ_1SR-mCh overexpression enhanced degradation of IP_3R proteins relative to that seen in control cells (Fig. 6*B*; 50.8 ± 14.1% in control cells, 77 ± 24.1% in σ_1R-mCh cells, and 16.3 ± 8.8% in σ_1SR-mCh cells at 24 h after tunicamycin treatment). Because σ_1SR-mCh overexpression promoted protein degradation, we examined the effects of σ_1SR-mCh overexpression on ER stress using stress markers, such as phosphorylation of PERK and its downstream target C/EBP homologous protein. As unexpected, neither PERK phosphorylation nor C/EBP homologous protein levels were enhanced by σ_1SR-mCh overexpression (Fig. 6*B*). However, when we evaluated autophagic responses based on production of the autophagy marker LC3-II, the ratio of LC3-II to total (LC3-I plus LC3-II) LC3 was markedly increased by 24 h after tunicamycin treatment (Fig. 6*B*).

σ_1SR Enhances Autophagosome Formation following ER Stress—Given that LC3-II production was enhanced in σ_1SR-mCh cells (Fig. 6*B*), we determined the diameters of vacuoles containing LC3-II (34). Twenty four hours after tunicamycin treatment, diameters of ~80% of LC3-positive vacuoles were smaller than the 1.0 μm seen in control cells (Fig. 7, *A* and *D*). σ_1R-mCh overexpression decreased the number of LC3-positive vacuoles compared with control without changing the size distribution (Fig. 7, *B*, *D* and *E*). By contrast, σ_1SR-mCh overexpression induced formation of larger autophagosomes than those seen in control cells, significantly shifting the size distribution profile. Over 50% of vacuoles were between 1.0 and 1.5 μm at 24 h after tunicamycin treatment (Fig. 7,*C* and *D*). The total number of LC3-positive particles also markedly increased in σ_1SR-mCh cells following tunicamycin treatment (Fig. 7*E*; 98.3 ± 11.4 in controls, 66.3 ± 7.2 in σ_1R-mCh cells, and 195 ± 16.7 in σ_1SR-mCh cells). The size of LC3-positive vacuoles did not change in control, σ_1R-mCh, and σ_1SR-mCh cells not treated with tunicamycin. Taken together, σ_1R overexpression inhibited formation of tunicamycin-induced autophagosomes, although σ_1SR overexpression promoted autophagosome formation under ER stress conditions.

σ_1SR Suppresses Mitochondrial ATP Production and Enhances Apoptosis following ER Stress—Finally, we asked how σ_1SR overexpression enhances the autophagic response. Because IP_3R-mediated Ca^{2+} transport into mitochondrial Ca^{2+} promotes oxidative phosphorylation, respiration, and ATP production by activating the tricarboxylic acid cycle (2, 35), we speculated that ATP production would be suppressed

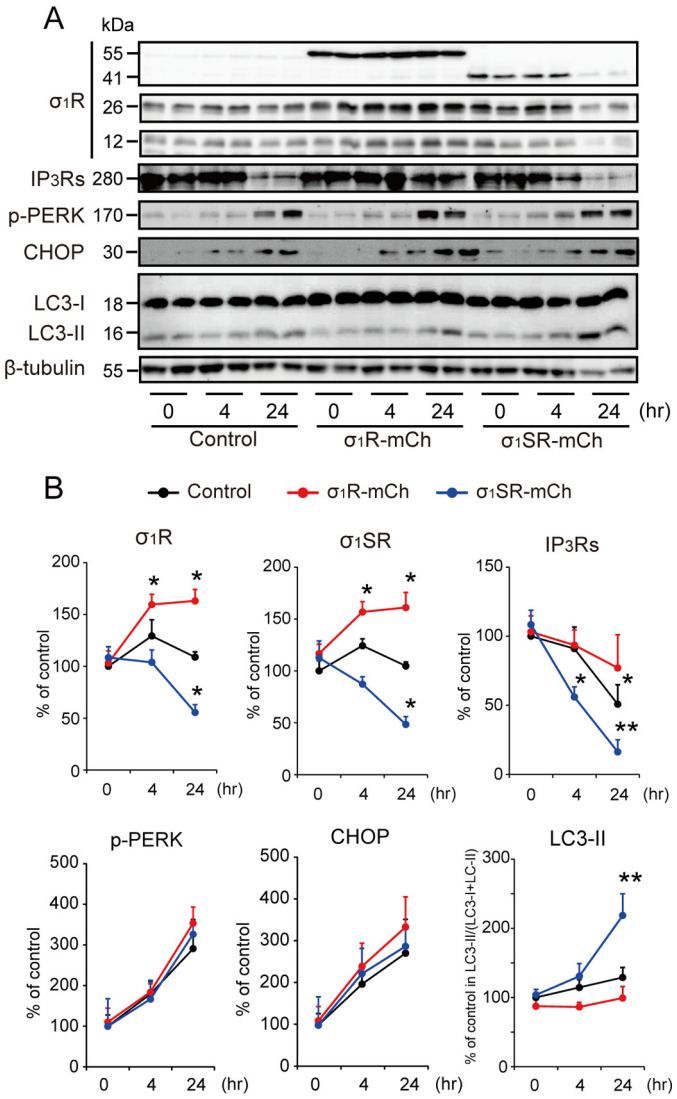

FIGURE 6. **σ_1SR enhances IP_3R destabilization following ER stress.** *A*, representative immunoblots probed with various antibodies are shown in control, σ_1R-mCh, and σ_1SR-mCh cells at 0, 4, and 24 h after 2 μg/ml tunicamycin treatment. *B*, quantitative densitometry analyses are shown. $n = 6$ per experiment. Each *bar* represents the mean ± S.E. *, $p < 0.05$; **, $p < 0.01$ *versus* control cells.

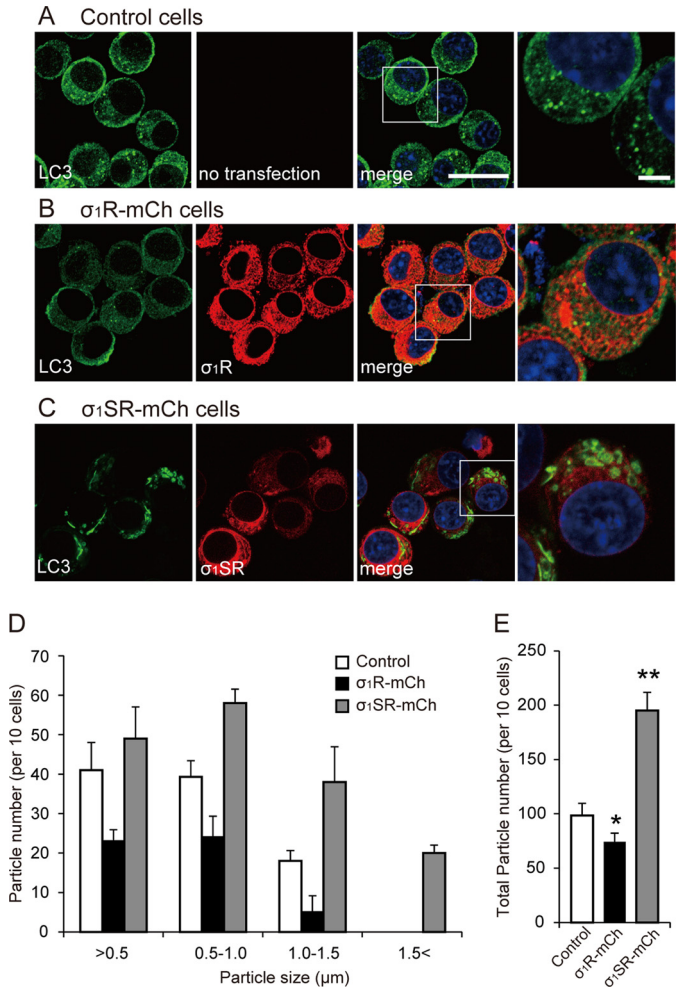

FIGURE 7. **σ_1SR enhances autophagosome formation following ER stress.** *A–C*, LC3 immunostaining in control (*A*), σ_1R-mCh (*B*), and σ_1SR-mCh (*C*) cells 24 h after 2 μg/ml tunicamycin treatment. *Enlarged images* indicate the *boxed areas*. *Scale bars*, 30 μm in low magnification and 10 μm in high magnification images. *D* and *E*, quantitative analysis of particle size (*D*) and total number (*E*) of LC3-immunoreactive autophagosomes 24 h after tunicamycin treatment. Ten fields (30 cells per field) in each condition were chosen randomly and photographed. Each *bar* represents the mean ± S.E. *, $p < 0.05$; **, $p < 0.01$ *versus* control cells.

by σ_1SR overexpression. Therefore, we measured changes in cellular ATP production with or without tunicamycin-induced ER stress. Unexpectedly, overexpression of σ_1R or σ_1SR markedly enhanced ATP production without tunicamycin treatment. In control cells, tunicamycin treatment significantly increased ATP production at 24 h but markedly suppressed it after 48 h of treatment. σ_1R overexpression significantly promoted ATP production both at 24 and 48 h after tunicamycin treatment (Fig. 8*A*). ATP production in σ_1SR-mCh cells was significantly suppressed at both the 24- and 48-h time points compared with control cells (Fig. 8*A*; 41.9 ± 1.1% in controls, 86.4 ± 5.3% in σ_1R-mCh cells, and 14.5 ± 0.24% in σ_1SR-mCh cells at 48 h compared with control cells at a resting state). To confirm that changes in ATP production are related to mitochondrial Ca^{2+} mobilization, we examined cellular ATP levels with or without tunicamycin treatment in the presence or absence of Ru360, a mitochondrial Ca^{2+} uptake blocker. ATP production enhanced by σ_1R or σ_1SR overexpression or by tunicamycin treatment was completely inhibited by Ru360 treatment (supplemental Fig. 3).

Because ATP production was suppressed 48 h after tunicamycin treatment and treatment could promote apoptosis, we evaluated apoptosis using TUNEL staining. σ_1SR-mCh overexpression significantly enhanced the number of TUNEL-positive cells 24 h after tunicamycin treatment, although σ_1R-mCh overexpression significantly suppressed tunicamycin-induced apoptosis. By contrast, σ_1SR-mCh overexpression markedly enhanced tunicamycin-induced apoptosis at 48 h (Fig. 8*B*; percentages of TUNEL-positive cells were 43.5 ± 8.4% in control, 19.1 ± 4.4% in σ_1R-mCh, and 70.4 ± 5.4% in σ_1SR-mCh).

To confirm that σ_1R-mCh and σ_1SR-mCh overexpression does not alter mitochondrial protein levels, we examined the expression of cytochrome *c* and the α subunit of ATP synthase (ATP5A1), subunits of the respiratory chain complex. σ_1R-mCh and σ_1SR-mCh cells showed no change in mRNA levels of

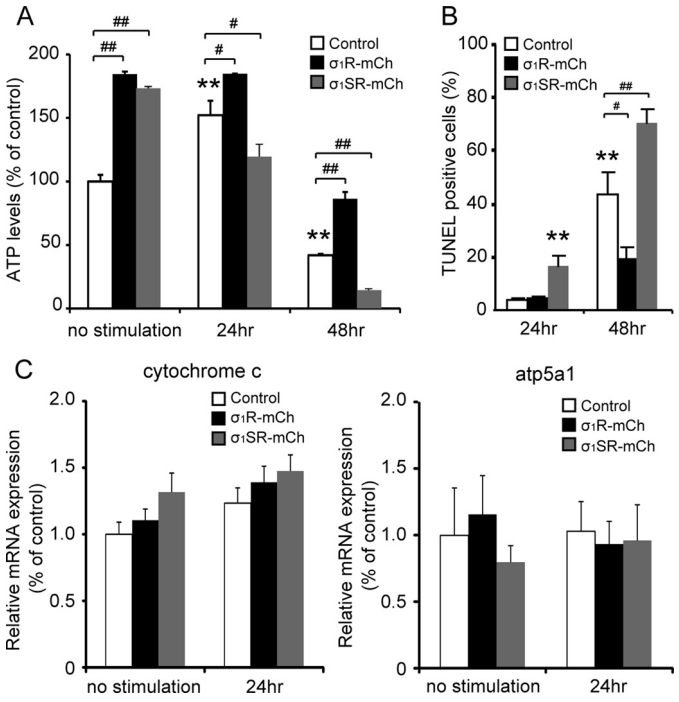

FIGURE 8. **σ_1SR suppresses mitochondrial ATP production and enhances apoptosis following ER stress.** *A,* intracellular ATP levels were measured in untreated cells or cells treated with 2 μg/ml tunicamycin at 24 and 48 h. *B,* TUNEL-positive cells were counted in treated cells at 24 and 48 h. One hundred cells from 13 randomly selected fields were counted in each experiment. *C,* real time PCR analysis showed that cytochrome *c* and ATP5A1 mRNA expression showed no significant differences between each group. $n = 6$ per experiment. Each *bar* represents the mean ± S.E. **, $p < 0.01$ *versus* control at no stimulation. #, $p < 0.05$; ##, $p < 0.01$ *versus* control at each time point.

these factors (Fig. 8*C*), indicating that σ_1R-mCh and σ_1SR-mCh overexpression does not interfere with mitochondrial structure or directly regulate IP_3R-mediated ATP production.

DISCUSSION

Here, we identified σ_1SR, a novel truncated isoform of the σ_1R. Using Neuro-2a cells, we showed that under physiological conditions the σ_1SR overexpression slightly stimulates ATP-induced cytosolic Ca^{2+} mobilization, in contrast with a small reduction promoted by σ_1R overexpression (Fig. 5*D*). These changes are likely due to increased and decreased Ca^{2+} mobilization into mitochondria induced by σ_1SR and σ_1R overexpression, respectively. Unexpectedly, σ_1SR overexpression increased ATP production in the absence of stress stimuli, such as ER stress (Fig. 8*A*), an activity not associated with reduction in ATP-induced mitochondrial Ca^{2+} mobilization. Thus, although ATP-induced mitochondrial Ca^{2+} mobilization is significantly reduced by σ_1SR overexpression, mitochondrial Ca^{2+} levels may be moderately increased with mitochondrial elongation. In support of this idea, increased ATP production seen following σ_1SR overexpression was eliminated by treating cells with the mitochondrial Ca^{2+} transport blocker Ru360 (supplemental Fig. 3).

Because basal ATP levels increase following overexpression of either isoform (Fig. 8*A*) and σ_1R overexpression in PC12 cells reportedly stimulates neurite sprouting in response to nerve growth factor (36), we hypothesized that σ_1SR overexpression might stimulate Neuro-2a cell differentiation. To evaluate this possibility, we measured morphological changes in both σ_1R- and σ_1SR-overexpressing Neuro-2a cells. Consistent with the findings of Ref. 36, σ_1R overexpression significantly stimulated neurite extension as compared with control cells. Similarly, like σ_1R overexpression, σ_1SR overexpression significantly stimulated neurite extension (supplemental Fig. 4; 3.2 ± 1.3% in control, 45.5 ± 4.3% in σ_1R, and 46 ± 7.4% in σ_1SR-transfected cells).

Mitochondrial elongation and extension of gap junctions between ER and mitochondria promoted by σ_1SR and σ_1R overexpression likely account for enhanced mitochondrial ATP production. Elongated mitochondria express higher levels of the dimeric form of ATPase, which is associated with more efficient ATP production (37). Increased contact space between the ER and mitochondria also likely enhances mitochondrial Ca^{2+} transport (38, 39). An ER-associated sorting protein, phosphofurin acidic cluster sorting protein 2 (PACS-2), is required for association of mitochondria with the ER. PACS-2 depletion induces mitochondrial fragmentation and uncoupling with the ER, resulting in aggravated ER stress (40). Mitofusin-2 (Mfn2) in the ER is also required for adhesion between mitochondrial and ER membranes. Depletion of Mfn2 impairs ER-mitochondrial Ca^{2+} transport (25) and induces cell death in cerebellar granule neurons (41). Taken together, σ_1R overexpression causes elongation of mitochondria and enhances IP_3R-induced Ca^{2+} transport, thereby promoting mitochondrial ATP production. Thus, elevated mitochondrial energy production likely promotes cell survival in the presence of ER stress.

σ_1SR Expression Promotes Mitochondrial ATP Depletion and Autophagy Only under ER Stress Conditions—The σ_1R reportedly stabilizes IP_3Rs to maintain Ca^{2+} transport from the ER into mitochondria in CHO cells (11). We confirmed that σ_1R overexpression enhances IP_3-induced mitochondrial Ca^{2+} transport and ATP production, whereas σ_1SR did not bind to IP_3Rs, and its overexpression did not enhance IP_3-induced mitochondrial Ca^{2+} transport. Under ER stress conditions, σ_1SR expression had detrimental effects on mitochondrial Ca^{2+} transport through the ER (Fig. 5*B*), promoting mitochondrial ATP depletion (Fig. 8). σ_1SR overexpression also destabilized IP_3Rs (Fig. 6*B*), which may account for decreased mitochondrial Ca^{2+} transport. Finally, σ_1SR overexpression promoted an autophagic response to ER stress following tunicamycin treatment without altering PERK activity (Figs. 6*B* and 7). Autophagy functions to recycle energy and nutrients in nutrient starvation and ER stress conditions (42), but the balance between autophagy and cell death is highly dependent on intracellular Ca^{2+} levels (43). IP_3R protein levels and activity are critical to inhibit autophagy (44). Indeed, autophagy is inhibited and promoted by IP_3R agonists (such as IP_3) and antagonists (such as xestospongins), respectively (45–47). In addition, IP_3R is required to inhibit autophagy under physiological conditions (6). The lack of mitochondrial Ca^{2+} transport by IP_3R depletion inhibits pyruvate dehydrogenase and increases the AMP/ATP ratio, thereby aggravating autophagy via AMP-activated protein kinase (6). IP_3Rs also inhibit autophagy through binding with Bcl-2 and Beclin-1 (known as autophagy-related gene 6) in HeLa cells (48). Inhibition of IP_3Rs

by xestospongin B promotes disruption of complexes formed by IP_3R, Bcl-2, and Beclin-1, activating autophagy. Taken together, IP_3R dysfunction through σ_1R down-regulation accounts for autophagic mechanisms in σ_1SR-expressed cells.

Physiological Relevance of Interaction between σ_1R and σ_1SR and Their Ligands—As shown in Fig. 1, the σ_1R is composed two transmembrane domains (TM1, amino acids 11–29; TM2, amino acids 91–109), an extracellular loop, and intracellular N and C termini with the C-terminal region including a large soluble domain (49, 50). Pharmacological studies indicate that numerous compounds, including benzomorphans (SKF-10047, pentazocine), antipsychotics (haloperidol), antidepressants (fluvoxamine), steroids (dehydroepiandrosterone, progesterone), and drugs of abuse (methamphetamine, cocaine) can bind to the σ_1R, primarily through the TM2 and C-terminal regions (50). The σ_1R agonist (+)-pentazocine positively modulates σ_1R/IP_3R association and stabilizes the complex at ER-mitochondria contact sites under ER stress. As a result, IP_3 binding to the IP_3R increases, and Ca^{2+} efflux is enhanced (11). In addition, ligand-induced regulation of this function apparently resides largely in the N terminus, contributing to functional coupling of C- and N-terminal σ_1R fragments. Wu and Bowen (51) reported that agonist binding to the σ_1R may change its conformation such that the N-terminal segment dissociates from the C terminus, which in turn can interact more avidly with IP_3R. Here, we showed that σ_1R binds to the IP_3R via its C terminus (Fig. 4). σ_1SR displays the opposite function, suppressing mitochondrial ATP production and promoting cell death following tunicamycin-induced ER stress. We suggest that σ_1SR, whose sequence is almost identical to the σ_1R N terminus (Fig. 1), interacts with the σ_1R C terminus, inhibiting σ_1R-mediated IP_3R-derived ER-mitochondrial Ca^{2+} transport.

Lymphocytes also express another σ_1R splice variant, which is replaced at Ala-13, Leu-28, and Ala-86 to Thr-13, Pro-28, and Val-86, respectively, and lacks 31 amino acids corresponding to residues 119–149 in the σ_1R protein (52). The σ_1R isoform lacks ligand binding sites. In NG108-15 cells, the full-length σ_1R forms a trimeric complex with the cytoskeletal adaptor protein ankyrin B and IP_3R in the ER membrane, and σ_1R agonists cause dissociation of ankyrin B from the IP_3R, promoting IP_3R activation (53). Indeed, the C-terminal σ_1R peptides (amino acids 102–223) transfected into MCF-7 breast tumor cells promote decreased levels of ankyrin B associated with the IP_3R compared with untransfected cells, enhancing IP_3R activation (51). In addition, the N-terminal σ_1R peptides (amino acids 1–100) expressed in MCF-7 cells weakly associate with ankyrin B and IP_3R complexes, but have little capacity to enhance IP_3R activity (51). In addition, a glutathione *S*-transferase (GST) fusion form of σ_1R (amino acids 116–223) has chaperone activity, blocking aggregation of denatured citrate synthase *in vitro*. However, GST-σ_1R (amino acids 29–92) lacks chaperone activity (11). Taken together with these studies, σ_1SR as defined here likely lacks chaperone activity and ligand binding ability and acts instead as a dominant negative form of σ_1R by blocking C-terminal chaperone activity under ER stress conditions or disrupting IP_3R/σ_1R interaction. However, under normal conditions, overexpression of either isoform promotes similar phenotypes relevant to ATP production,

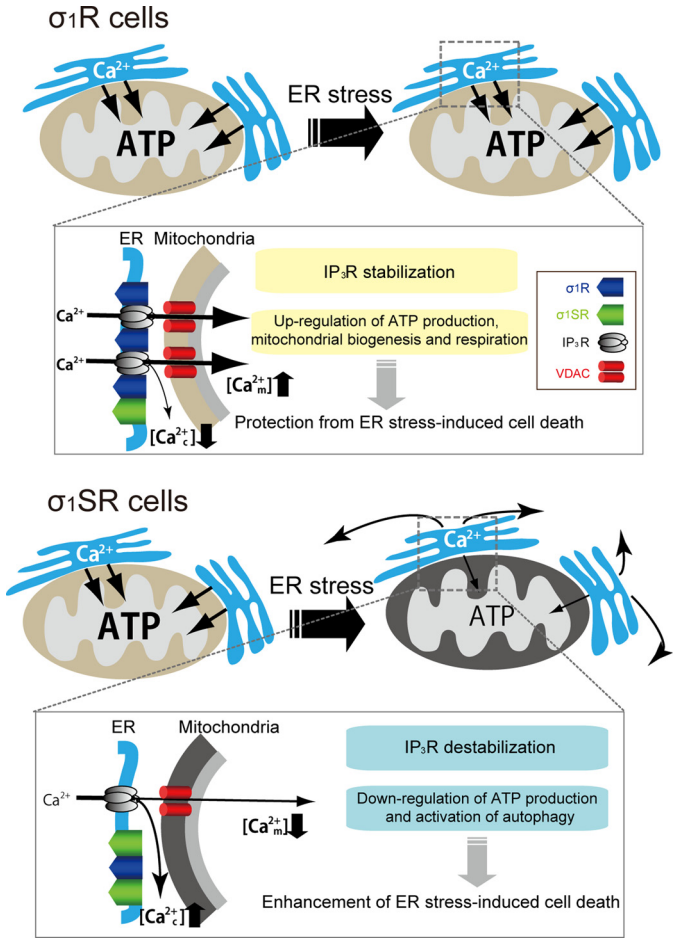

FIGURE 9. **Schematic representation of altered mitochondrial ATP production and cell death in the presence of two σ_1R isoforms following ER stress.** *Upper,* in ER stress conditions, σ_1R stabilizes IP_3Rs and sustains mitochondrial Ca^{2+} uptake-derived ATP production, enhancing survival. *Lower,* by contrast, σ_1SR expression destabilizes IP_3Rs and promotes dysfunction of IP_3R-derived ER-mitochondrial Ca^{2+} transfer through functional loss of σ_1R, resulting in ATP depletion and autophagic apoptosis. In resting conditions, both σ_1R isoforms positively regulate mitochondrial biogenesis.

mitochondrial elongation, and neurite extension, suggesting that endogenous σ_1SR has an alternate unique function in mitochondrial elongation and adhesion with the ER.

We showed that ATP-induced $[Ca^{2+}]_c$ mobilization in σ_1SR-mCh cells was greater than that seen in control cells in Ca^{2+}-free Krebs buffer (Fig. 5*D*). σ_1SR expression possibly destabilizes IP_3Rs by inhibiting chaperone activity of endogenous σ_1R, thereby reducing IP_3R-derived ER-mitochondrial Ca^{2+} transport (Fig. 9). This activity may elicit enhanced $[Ca^{2+}]_c$ mobilization following ATP stimulation of σ_1SR-mCh cells. However, extensive studies are required to define how IP_3R/σ_1R interaction is disrupted by σ_1SR overexpression.

Among the three IP_3R isoforms, type-3 IP_3R plays a critical role in induction of apoptosis by preferentially transmitting Ca^{2+} signals into mitochondria (54). siRNA-based knockdown of type-3 IP_3R significantly decreases IP_3-induced mitochondrial Ca^{2+} concentrations in CHO cells, whereas knockdown of type-1 IP_3R reduces cytosolic Ca^{2+} concentration (54). In addition, type-3 IP_3Rs are particularly enriched at the MAM, whereas type-1 IP_3R is homogeneously expressed in ER membranes in neurons (9). σ_1Rs form a trimeric complex with

ankyrin-B and the type-3 IP_3Rs but not with type-1 IP_3Rs in NG108-15 cells (53). Taken together, σ_1R acts as a specific chaperone for type-3 IP_3R at the MAM, regulating $[Ca^{2+}]_{mt}$ mobilization in neurons. Notably, σ_1R agonists, including (+)-pentazocine, increase $[Ca^{2+}]_c$ from the ER following bradykinin stimulation of NG108-15 cells (55). In addition, σ_1R (amino acids 102–223)-transfected MCF-7 cells also show increased $[Ca^{2+}]_c$ induced by bradykinin stimulation (51), suggesting that other σ_1R-binding proteins regulate intracellular Ca^{2+} mobilization. In the future, we will investigate whether these binding proteins regulate $[Ca^{2+}]_c$ mobilization after stimulation with σ_1R ligands in neurons and define σ_1SR function in $[Ca^{2+}]$ mobilization.

Pathophysiological Relevance of σ_1SR—Autophagy is activated in several neurodegenerative disorders, although its significance in neuronal death and survival remains to be defined (56). Al-Saif *et al.* (19) reported a *SIGMAR1* missense mutation in exon 2 associated with juvenile amyotrophic lateral sclerosis (c.304G→C) that substitutes glutamine for glutamic acid at residue 102 (E102Q), which occurs at the σ_1SR splice site (Fig. 1). Expression of the E102Q mutant enhances apoptosis in the mouse motor neuron-like cell line NSC34 (19). Further studies are needed to reveal functions of σ_1SR in neurodegenerative disorders.

In conclusion, we have identified a novel σ_1R isoform, σ_1SR, as a key molecule in ER stress-related cellular apoptosis through regulation of ER-mediated mitochondrial biogenesis. Importantly, σ_1SR does not bind IP_3Rs but inhibits the ability of σ_1R to promote mitochondrial ATP production through IP_3R-mediated Ca^{2+} transport. Future studies should address pathological conditions in which σ_1SR is up-regulated and potential interference with σ_1R and mitochondrial function.

Acknowledgments—We thank Dr. Teruo Hayashi of the National Institute on Drug Abuse, Department of Health and Human Services, for kindly providing antibodies against the N and C termini of σ_1R; Dr. Akihiko Tanimura and Dr. Yosuke Tojyo in the Department of Pharmacology, School of Dentistry, Health Sciences University of Hokkaido, for helpful advice on Ca^{2+} imaging analysis; and Dr. Atsushi Miyawaki at the Brain Science Institute, RIKEN, for kindly providing ratiometric pericam-mt/pcDNA3.

REFERENCES

1. Robb-Gaspers, L. D., Burnett, P., Rutter, G. A., Denton, R. M., Rizzuto, R., and Thomas, A. P. (1998) Integrating cytosolic calcium signals into mitochondrial metabolic responses. *EMBO J.* **17,** 4987–5000
2. Csordás, G., Renken, C., Várnai, P., Walter, L., Weaver, D., Buttle, K. F., Balla, T., Mannella, C. A., and Hajnóczky, G. (2006) Structural and functional features and significance of the physical linkage between ER and mitochondria. *J. Cell Biol.* **174,** 915–921
3. Rizzuto, R., Brini, M., Murgia, M., and Pozzan, T. (1993) Microdomains with high Ca^{2+} close to IP_3-sensitive channels that are sensed by neighboring mitochondria. *Science* **262,** 744–747
4. Rizzuto, R., Pinton, P., Carrington, W., Fay, F. S., Fogarty, K. E., Lifshitz, L. M., Tuft, R. A., and Pozzan, T. (1998) Close contacts with the endoplasmic reticulum as determinants of mitochondrial Ca^{2+} responses. *Science* **280,** 1763–1766
5. Hanson, C. J., Bootman, M. D., and Roderick, H. L. (2004) Cell signaling. IP_3 receptors channel calcium into cell death. *Curr. Biol.* **14,** R933-R935
6. Cárdenas, C., Miller, R. A., Smith, I., Bui, T., Molgó, J., Müller, M., Vais, H., Cheung, K. H., Yang, J., Parker, I., Thompson, C. B., Birnbaum, M. J., Hallows, K. R., and Foskett, J. K. (2010) Essential regulation of cell bioenergetics by constitutive $InsP_3$ receptor Ca^{2+} transfer to mitochondria. *Cell* **142,** 270–283
7. Vance, J. E. (1990) Phospholipid synthesis in a membrane fraction associated with mitochondria. *J. Biol. Chem.* **265,** 7248–7256
8. Giorgi, C., De Stefani, D., Bononi, A., Rizzuto, R., and Pinton, P. (2009) Structural and functional link between the mitochondrial network and the endoplasmic reticulum. *Int. J. Biochem. Cell Biol.* **41,** 1817–1827
9. Hayashi, T., Rizzuto, R., Hajnoczky, G., and Su, T. P. (2009) MAM. More than just a housekeeper. *Trends Cell Biol.* **19,** 81–88
10. Hanner, M., Moebius, F. F., Flandorfer, A., Knaus, H. G., Striessnig, J., Kempner, E., and Glossmann, H. (1996) Purification, molecular cloning, and expression of the mammalian σ1-binding site. *Proc. Natl. Acad. Sci. U.S.A.* **93,** 8072–8077
11. Hayashi, T., and Su, T. P. (2007) σ1 receptor chaperones at the ER-mitochondrion interface regulate Ca^{2+} signaling and cell survival. *Cell* **131,** 596–610
12. Hayashi, T., and Su, T. P. (2003) σ1 receptors (σ_1-binding sites) form raft-like microdomains and target lipid droplets on the endoplasmic reticulum. Roles in endoplasmic reticulum lipid compartmentalization and export. *J. Pharmacol. Exp. Ther.* **306,** 718–725
13. Martina, M., Turcotte, M. E., Halman, S., and Bergeron, R. (2007) The σ1 receptor modulates NMDA receptor synaptic transmission and plasticity via SK channels in rat hippocampus. *J. Physiol.* **578,** 143–157
14. Celsi, F., Pizzo, P., Brini, M., Leo, S., Fotino, C., Pinton, P., and Rizzuto, R. (2009) Mitochondria, calcium, and cell death. A deadly triad in neurodegeneration. *Biochim. Biophys. Acta* **1787,** 335–344
15. Maurice, T., and Lockhart, B. P. (1997) Neuroprotective and anti-amnesic potentials of σ receptor ligands. *Prog. Neuropsychopharmacol. Biol. Psychiatry* **21,** 69–102
16. Urani, A., Romieu, P., Roman, F. J., Yamada, K., Noda, Y., Kamei, H., Manh Tran, H., Nagai, T., Nabeshima, T., and Maurice, T. (2004) Enhanced antidepressant efficacy of σ1 receptor agonists in rats after chronic intracerebroventricular infusion of β-amyloid-(1–40) protein. *Eur. J. Pharmacol.* **486,** 151–161
17. Schetz, J. A., Perez, E., Liu, R., Chen, S., Lee, I., and Simpkins, J. W. (2007) A prototypical σ1 receptor antagonist protects against brain ischemia. *Brain Res.* **1181,** 1–9
18. Luty, A. A., Kwok, J. B., Dobson-Stone, C., Loy, C. T., Coupland, K. G., Karlström, H., Sobow, T., Tchorzewska, J., Maruszak, A., Barcikowska, M., Panegyres, P. K., Zekanowski, C., Brooks, W. S., Williams, K. L., Blair, I. P., Mather, K. A., Sachdev, P. S., Halliday, G. M., and Schofield, P. R. (2010) σ nonopioid intracellular receptor 1 mutations cause frontotemporal lobar degeneration-motor neuron disease. *Ann. Neurol.* **68,** 639–649
19. Al-Saif, A., Al-Mohanna, F., and Bohlega, S. (2011) A mutation in σ1 receptor causes juvenile amyotrophic lateral sclerosis. *Ann. Neurol.* **70,** 913–919
20. Shioda, N., Yamamoto, Y., Watanabe, M., Binas, B., Owada, Y., and Fukunaga, K. (2010) Heart-type fatty acid-binding protein regulates dopamine D_2 receptor function in mouse brain. *J. Neurosci.* **30,** 3146–3155
21. Tagashira, H., Bhuiyan, S., Shioda, N., Hasegawa, H., Kanai, H., and Fukunaga, K. (2010) σ1 receptor stimulation with fluvoxamine ameliorates transverse aortic constriction-induced myocardial hypertrophy and dysfunction in mice. *Am. J. Physiol. Heart. Circ. Physiol.* **299,** H1535–H1545
22. Takeuchi, Y., and Fukunaga, K. (2003) Differential subcellular localization of two dopamine D_2 receptor isoforms in transfected NG108-15 cells. *J. Neurochem.* **85,** 1064–1074
23. Shioda, N., Moriguchi, S., Shirasaki, Y., and Fukunaga, K. (2006) Generation of constitutively active calcineurin by calpain contributes to delayed neuronal death following mouse brain ischemia. *J. Neurochem.* **98,** 310–320
24. Shioda, N., Beppu, H., Fukuda, T., Li, E., Kitajima, I., and Fukunaga, K. (2011) Aberrant calcium/calmodulin-dependent protein kinase II (CaMKII) activity is associated with abnormal dendritic spine morphology in the ATRX mutant mouse brain. *J. Neurosci.* **31,** 346–358
25. de Brito, O. M., and Scorrano, L. (2008) Mitofusin 2 tethers endoplasmic reticulum to mitochondria. *Nature* **456,** 605–610

26. Manders, E. M., Verbeek, F. J., and Aten, J. A. (1993) Measurement of co-localization of objects in dual color confocal images. *J. Microsc.* **169,** 375–382
27. Tanimura, A., and Turner, R. J. (1996) Inositol 1,4,5-trisphosphate-dependent oscillations of luminal [Ca^{2+}] in permeabilized HSY cells. *J. Biol. Chem.* **271,** 30904–30908
28. Shioda, N., Han, F., Morioka, M., and Fukunaga, K. (2008) Bis(1-oxy-2-pyridinethiolato)oxovanadium(IV) enhances neurogenesis via phosphatidylinositol 3-kinase/Akt and extracellular signal-regulated kinase activation in the hippocampal subgranular zone after mouse focal cerebral ischemia. *Neuroscience* **155,** 876–887
29. Su, T. P., London, E. D., and Jaffe, J. H. (1988) Steroid binding at σ receptors suggests a link between endocrine, nervous, and immune systems. *Science* **240,** 219–221
30. Hellewell, S. B., Bruce, A., Feinstein, G., Orringer, J., Williams, W., and Bowen, W. D. (1994) Rat liver and kidney contain high densities of σ1 and σ2 receptors. Characterization by ligand binding and photoaffinity labeling. *Eur. J. Pharmacol.* **268,** 9–18
31. Kekuda, R., Prasad, P. D., Fei, Y. J., Leibach, F. H., and Ganapathy, V. (1996) Cloning and functional expression of the human type 1 σ receptor (hσR1). *Biochem. Biophys. Res. Commun.* **229,** 553–558
32. Seth, P., Leibach, F. H., and Ganapathy, V. (1997) Cloning and structural analysis of the cDNA and the gene encoding the murine type 1 σ receptor. *Biochem. Biophys. Res. Commun.* **241,** 535–540
33. Nagai, T., Sawano, A., Park, E. S., and Miyawaki, A. (2001) Circularly permuted green fluorescent proteins engineered to sense Ca^{2+}. *Proc. Natl. Acad. Sci. U.S.A.* **98,** 3197–3202
34. Kabeya, Y., Mizushima, N., Ueno, T., Yamamoto, A., Kirisako, T., Noda, T., Kominami, E., Ohsumi, Y., and Yoshimori, T. (2000) LC3, a mammalian homologue of yeast Apg8p, is localized in autophagosome membranes after processing. *EMBO J.* **19,** 5720–5728
35. Hajnóczky, G., Csordás, G., Krishnamurthy, R., and Szalai, G. (2000) Mitochondrial calcium signaling driven by the IP_3 receptor. *J. Bioenerg. Biomembr.* **32,** 15–25
36. Takebayashi, M., Hayashi, T., and Su, T. P. (2002) Nerve growth factor-induced neurite sprouting in PC12 cells involves σ1 receptors. Implications for antidepressants. *J. Pharmacol. Exp. Ther.* **303,** 1227–1237
37. Strauss, M., Hofhaus, G., Schröder, R. R., and Kühlbrandt, W. (2008) Dimer ribbons of ATP synthase shape the inner mitochondrial membrane. *EMBO J.* **27,** 1154–1160
38. Bernardi, P. (1999) Mitochondrial transport of cations. Channels, exchangers, and permeability transition. *Physiol. Rev.* **79,** 1127–1155
39. Green, D. R., and Kroemer, G. (2004) The pathophysiology of mitochondrial cell death. *Science* **305,** 626–629
40. Simmen, T., Aslan, J. E., Blagoveshchenskaya, A. D., Thomas, L., Wan, L., Xiang, Y., Feliciangeli, S. F., Hung, C. H., Crump, C. M., and Thomas, G. (2005) PACS-2 controls endoplasmic reticulum-mitochondria communication and Bid-mediated apoptosis. *EMBO J.* **24,** 717–729
41. Jahani-Asl, A., Cheung, E. C., Neuspiel, M., MacLaurin, J. G., Fortin, A., Park, D. S., McBride, H. M., and Slack, R. S. (2007) Mitofusin 2 protects cerebellar granule neurons against injury-induced cell death. *J. Biol. Chem.* **282,** 23788–23798
42. Klionsky, D. J. (2007) Autophagy. From phenomenology to molecular understanding in less than a decade. *Nat. Rev. Mol. Cell Biol.* **8,** 931–937
43. Debnath, J., Baehrecke, E. H., and Kroemer, G. (2005) Does autophagy contribute to cell death? *Autophagy* **1,** 66–74
44. Decuypere, J. P., Monaco, G., Bultynck, G., Missiaen, L., De Smedt, H., and Parys, J. B. (2011) The IP_3 receptor-mitochondria connection in apoptosis and autophagy. *Biochim. Biophys. Acta* **1813,** 1003–1013
45. Sarkar, S., Floto, R. A., Berger, Z., Imarisio, S., Cordenier, A., Pasco, M., Cook, L. J., and Rubinsztein, D. C. (2005) Lithium induces autophagy by inhibiting inositol monophosphatase. *J. Cell Biol.* **170,** 1101–1111
46. Criollo, A., Maiuri, M. C., Tasdemir, E., Vitale, I., Fiebig, A. A., Andrews, D., Molgó, J., Díaz, J., Lavandero, S., Harper, F., Pierron, G., di Stefano, D., Rizzuto, R., Szabadkai, G., and Kroemer, G. (2007) Regulation of autophagy by the inositol trisphosphate receptor. *Cell Death. Differ.* **14,** 1029–1039
47. Criollo, A., Vicencio, J. M., Tasdemir, E., Maiuri, M. C., Lavandero, S., and Kroemer, G. (2007) The inositol trisphosphate receptor in the control of autophagy. *Autophagy* **3,** 350–353
48. Vicencio, J. M., Ortiz, C., Criollo, A., Jones, A. W., Kepp, O., Galluzzi, L., Joza, N., Vitale, I., Morselli, E., Tailler, M., Castedo, M., Maiuri, M. C., Molgó, J., Szabadkai, G., Lavandero, S., and Kroemer, G. (2009) The inositol 1,4,5-trisphosphate receptor regulates autophagy through its interaction with Beclin-1. *Cell Death. Differ.* **16,** 1006–1017
49. Aydar, E., Palmer, C. P., Klyachko, V. A., and Jackson, M. B. (2002) The σ receptor as a ligand-regulated auxiliary potassium channel subunit. *Neuron* **34,** 399–410
50. Su, T. P., Hayashi, T., Maurice, T., Buch, S., and Ruoho, A. E. (2010) The σ1 receptor chaperone as an inter-organelle signaling modulator. *Trends Pharmacol. Sci.* **31,** 557–566
51. Wu, Z., and Bowen, W. D. (2008) Role of σ1 receptor C-terminal segment in inositol 1,4,5-trisphosphate receptor activation. Constitutive enhancement of calcium signaling in MCF-7 tumor cells. *J. Biol. Chem.* **283,** 28198–28215
52. Ganapathy, M. E., Prasad, P. D., Huang, W., Seth, P., Leibach, F. H., and Ganapathy, V. (1999) Molecular and ligand-binding characterization of the σ receptor in the Jurkat human T lymphocyte cell line. *J. Pharmacol. Exp. Ther.* **289,** 251–260
53. Hayashi, T., and Su, T. P. (2001) Regulating ankyrin dynamics. Roles of σ1 receptors. *Proc. Natl. Acad. Sci. U.S.A.* **98,** 491–496
54. Mendes, C. C., Gomes, D. A., Thompson, M., Souto, N. C., Goes, T. S., Goes, A. M., Rodrigues, M. A., Gomez, M. V., Nathanson, M. H., and Leite, M. F. (2005) The type III inositol 1,4,5-trisphosphate receptor preferentially transmits apoptotic Ca^{2+} signals into mitochondria. *J. Biol. Chem.* **280,** 40892–40900
55. Hayashi, T., Maurice, T., and Su, T. P. (2000) Ca^{2+} signaling via σ_1-receptors. Novel regulatory mechanism affecting intracellular Ca^{2+} concentration. *J. Pharmacol. Exp. Ther.* **293,** 788–798
56. Nixon, R. A. (2006) Autophagy in neurodegenerative disease. Friend, foe, or turncoat? *Trends Neurosci.* **29,** 528–535